Ultralow temperature synthesis and densification of $Ag_2CaV_4O_{12}$ with improved microwave dielectric performances

Chunchun Li[1, 2*], Changzhi Yin[1], Jibran Khaliq[3], Laijun Liu[1]

[1]*Guangxi universities key laboratory of non-ferrous metal oxide electronic functional materials and devices, College of Material Science and Engineering, Guilin University of Technology, Guilin, 541004, China*

[2]*School of Materials Science and Engineering, Nanchang University, Nanchang 330031, People's Republic of China*

[3]*Department of Mechanical and Construction Engineering, Faculty of Engineering and Environment, Northumbria University at Newcastle, NE1 8ST, UK*

Abstract

At extremely low temperatures, $Ag_2CaV_4O_{12}$ was easily synthesised using the traditional solid-state approach. With a low relative permittivity (ε_r) of 7.52 and a high quality factor (Qxf) of 48,800 GHz (f = 13.6 GHz) and a temperature coefficient of resonance frequency (τ_f) of -77.4 ppm/°C, dense ceramics sintered at 480 °C with outstanding microwave dielectric characteristics were attained. By combining with rutile TiO_2, a composite ceramic with balanced microwave dielectric properties (τ_f = 3.2 ppm/°C, ε_r = 10.96, and $Q \times f$ = 49,081 GHz) were achieved. No chemical reaction between $Ag_2CaV_4O_{12}$ and silver and aluminum occurred. All of the findings show that $Ag_2CaV_4O_{12}$ has the potential to be used as dielectric resonances in wireless communications and as substrates in low-temperature cofired ceramics. Furthermore, the processing at an ultralow temperature of $Ag_2CaV_4O_{12}$ shows that it is extraordinarily energy saving from the point of view of fabrication and might allow for room-temperature synthesis by combining with high-energy mechanical milling or sintering using high pressure such as hot isostatic pressing (HIP), spark plasma sintering (SPS), and cold sintering (CS).

Keywords: Ceramics; Dielectric properties; Low-temperature synthesis; Low-temperature cofired ceramics

* Authors to whom correspondence should be addressed: lichunchun2003@126.com;

Introduction

Due to their extensive applications in dielectric resonances, filters, oscillators, and antennas, microwave dielectric materials have been regarded as the main components in wireless communication [1-3]. The Internet of Things (IoT) and 5th generation telecommunications have increased the demand for microwave dielectric materials in recent years[4-6]. Among them, miniaturization is still an indispensable demand which is driving the manufacturing of microwave dielectric materials. High permittivity (ε_r) is considered advantageous to achieve miniaturization [1] as the device size is directly proportional to $\varepsilon_r^{-1/2}$. High dielectric loss and a substantial temperature coefficient of permittivity are prevalent in high permittivity materials [7-9], compromising frequency selection and thermal stability and restricting their practical applications. On the other hand, the multilayer cofired ceramic technologies provide viable miniaturization solutions by paralleling the dielectric tapes layer by layer to gain equivalently high permittivity. In this respect, the manufacturing of modern microwave devices relies heavily on low-temperature cofired ceramic technology (LTCC) [2, 10-11]. The dielectric materials utilized in these technologies should have appropriate dielectric properties and chemical compatibility with electrodes (such as Cu and Ag) [10]. Sintering temperatures lower than the melting points of the electrodes (e.g., 1084 °C for copper) are one of the success criteria for LTCC ceramics so they can be co-fired with the electrodes. To lower the sintering temperature of LTCC microwave ceramics, glasses or oxides having low melting points are added. The recent proposition of inexpensive aluminum electrodes (with a melting point ~ 660 °C) to replace silver and copper has prompted the emergence and rapid development of the so-called ULTCC (ultra-low temperature cofired ceramic). The sintering temperatures in ULTCC are generally lower than 700 °C to achieve consolidation and avoid electrode melting. The shift from LTCC to ULTCC poses a new challenge to discover new materials that can be

sintered below 700°C and have good chemical compatibility with Al.

To date, some materials with low sintering temperatures (around 700 °C) have been synthesized, the bulk of which are tungstates, tellurates, vanadates, molybdates, together with various alloying additions such as Li, Na, and K [12-17]. For LTCC applications, several combinations of the above-mentioned chemicals have been studied. Out of those systems, the Ag_2O-CaO-V_2O_5 system is the most appealing because it has two low-melting-point constituents, making it an attractive choice for a low-firing material system for ULTCC. Interestingly, only one compound $Ag_2CaV_4O_{12}$ exists in the Ag_2O-CaO-V_2O_5 system according to the phase diagram. Researchers mainly focused on optical and photocatalytic properties of $Ag_2CaV_4O_{12}$ [18], while the dielectric properties have not been studied before to the best of our knowledge.

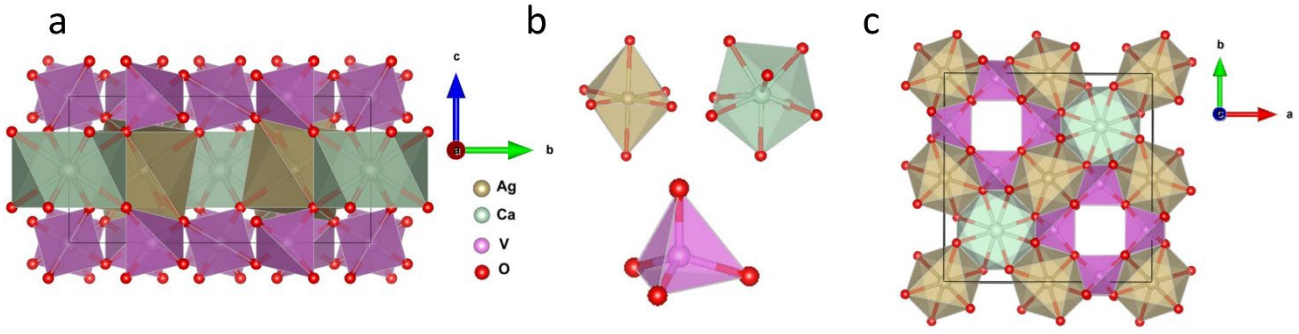

Figure 1

The crystal structure of $Ag_2CaV_4O_{12}$ is depicted in **Figure 1 (a-c)**, along with the corresponding coordinated polyhedral with oxygen. There are three different types of polyhedra: (i) V^{5+} cations are four-coordinated with oxygen via corner-sharing to form a tetrahedron. Four such corner-sharing VO_4 tetrahedra formed a hollow channel along the *c*-axis. (ii) Ag^+ cations are six-coordinated with oxygen forming an octahedron that separates from each other but is connected with the adjacent tetrahedra via edge-sharing. (iii) Ca^{2+} cations are eight-coordinated with oxygen forming a dodecahedron, which is corner-connected with the tetrahedron (VO_4) and edge-connected with the octahedron (AgO_6). As a

result, it enticed us for the first time to investigate the microwave dielectric and low sintering temperatures of $Ag_2CaV_4O_{12}$.

We developed a novel ultralow-temperature-firing ceramic, $Ag_2CaV_4O_{12}$, based on these factors, and investigated its potential applicability in ULTCC technology. In the microwave frequency regime, the sintering behavior and structure-property relationship were examined, together with the chemical compatibility with aluminum and silver.

Experimental procedures

Ag_2O, $CaCO_3$, and V_2O_5 (all reagents have a purity of 99.9%) were used as raw materials to synthesize $Ag_2CaV_4O_{12}$ ceramics through a conventional solid-state sintering route. The raw materials were weighed depending upon the stoichiometric ratio and mixed using ethyl alcohol and ZrO_2 balls in nylon containers for 6 h in a planetary ball mill. After milling, the slurries were kept at 120 °C to dry followed by calcination at 300 °C for 6 hours. After calcination, the powders were re-milled to break the agglomerates and 5 wt.% PVA was added as a binder as a sintering aid. Finally, the mixture was cold pressed into pellets having Φ10×6.5 mm under 10 MPa. To optimize the densification of $Ag_2CaV_4O_{12}$ the sintering process was carried out in the temperature range from 420-500 °C with an increment of 20 °C.

Archimedes' principle was used to measure the bulk density of sintered ceramic. The crystal structure and phase purity were analyzed using X-ray diffraction (CuKα1, 1.54059 Å, Model X'Pert PRO, PANalytical, Almelo, Holland). The relative density can be calculated as follow:

$$\rho_{re} = \frac{\rho_{mea}}{\rho_{th}} \times 100\% \qquad (1)$$

where, the ρ_{mea} represents the bulk density obtained via the Archimedes principle, and the ρ_{th} is the

theoretical density that is calculated based on the XRD data. High-resolution transmission electron microscopy (HRTEM) (JEM-2100F) at an accelerating voltage of 200 kV was used together with selected area electron diffraction (SAED) to analyze the samples. Filed emission scanning electron microscope (FE-SEM).was used to examine the surface morphologies of the samples. The dielectric properties such as relative permittivity (ε_r), quality factor ($Q\times f$) at microwave frequency, the temperature coefficient of resonant frequency (τ_f), and IR spectra were measured using the techniques mentioned in our earlier reports.[19]

Results and discussion

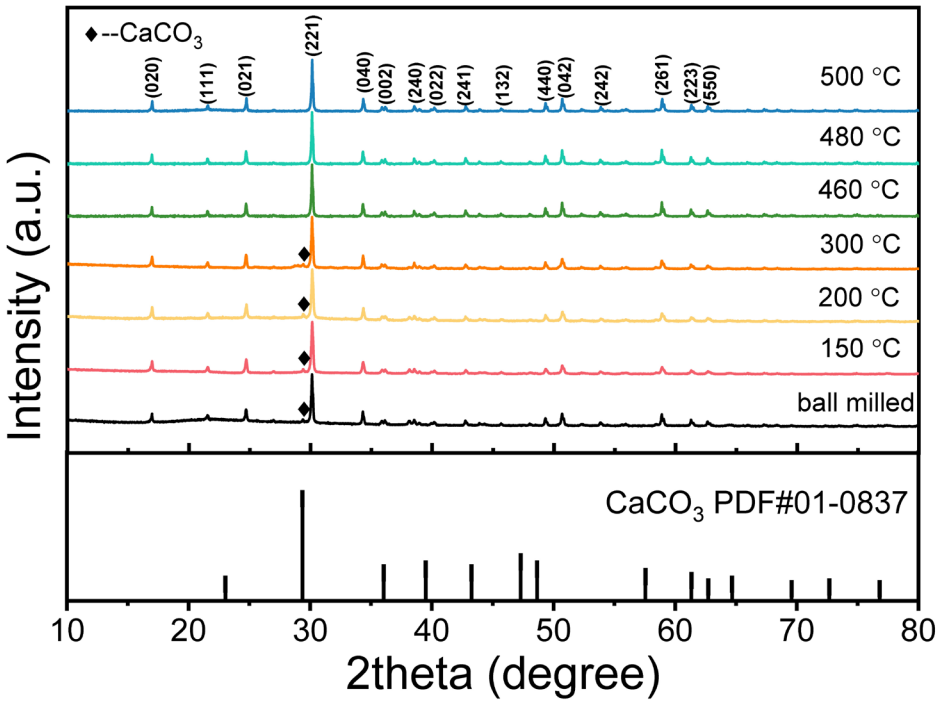

Figure 2

XRD spectra of the powders calcined at various temperatures (from 150-500 °C) are shown in Figure 2. For comparison, the XRD pattern of the ball-milled sample is also shown. Interestingly, the ball-mixed precursors (uncalcined) contained $Ag_2CaV_4O_{12}$ as a dominant phase (JCPDS No. 42-0095) with minor unreacted $CaCO_3$. This is unexpected but might origin from the driving force (like frictional

and gravitational force, heat effect) from ball milling caused by high rotate speed. To rule out the high energy offered by ball milling and get deep insight into the phase formation of $Ag_2CaV_4O_{12}$, a comparative experiment was designed via hand grinding of the raw materials. As shown in Supplementary information Figure S1, the hand-ground powders with low-temperature heat treatment (at 50 ºC, 100 ºC, and 150 ºC) formed the $Ag_2CaV_4O_{12}$ phase. $Ag_2CaV_4O_{12}$ can be formed just via ball milling and low-temperature heating after hand grinding, revealing its low reaction entropy.

With increasing the calcination temperature, diffraction intensities of $CaCO_3$ decreased and completely disappeared at 460 ºC and, single-phase $Ag_2CaV_4O_{12}$ with a tetragonal space group *P4/nbm* was detected. No variation in XRD profiles was observed as the temperature was further increased to 500ºC. Moreover, the high similarity of Raman spectra (Supplementary information Figure S2) for the samples sintered in the range of 420 to 500 ºC suggested the structural stability of $Ag_2CaV_4O_{12}$.

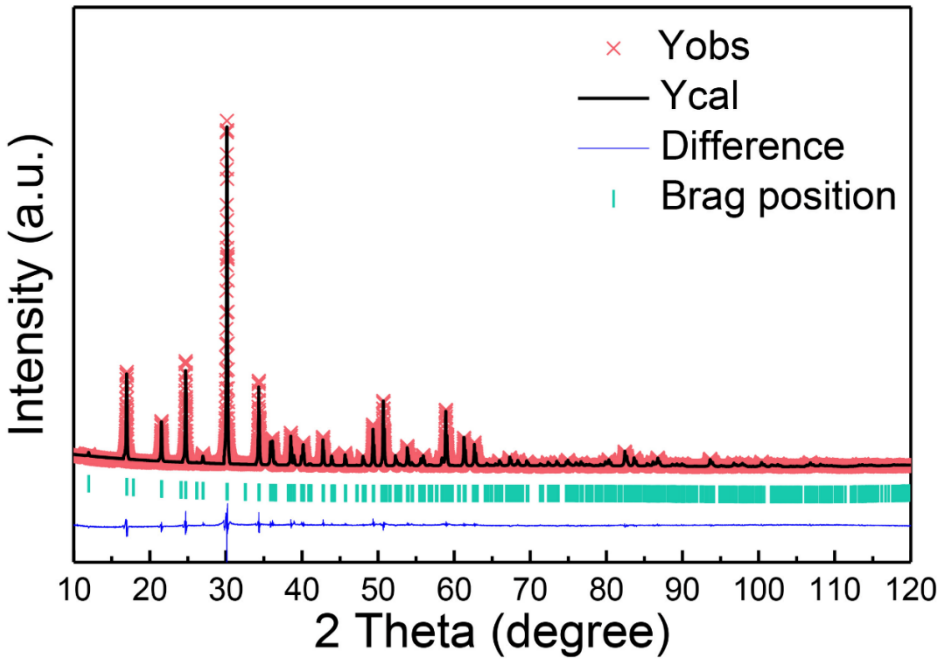

Figure 3

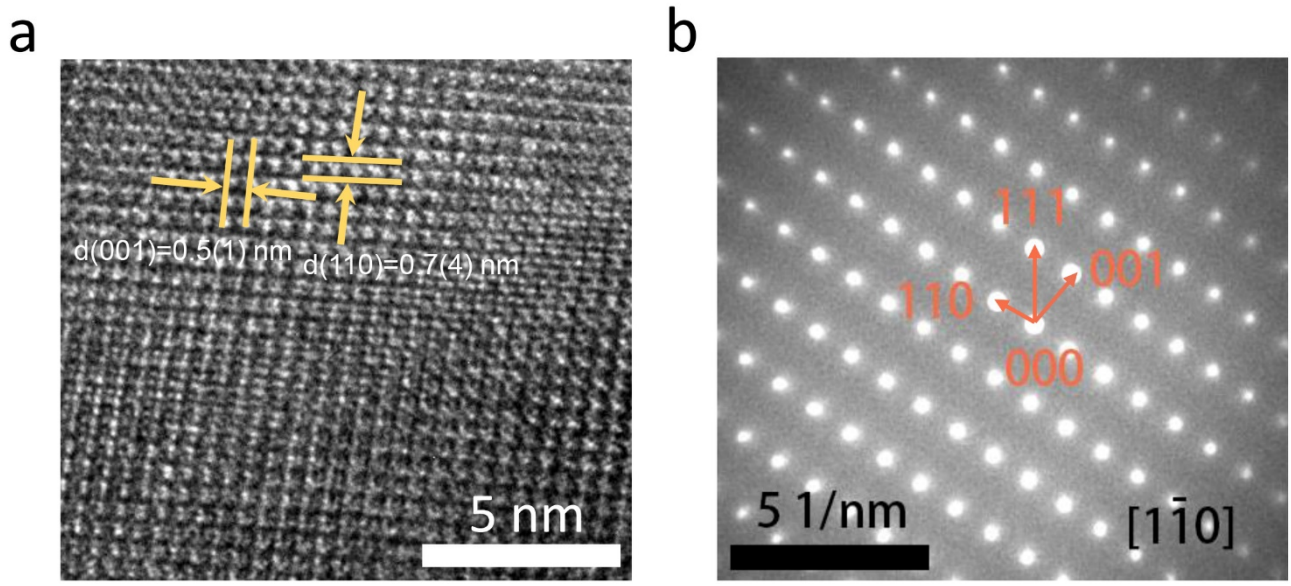

Figure 4

To improve crystal structure analysis and better comprehend phase purity, Rietveld refinement was applied to XRD data of the sample sintered at 480 °C. The zero shift, background, scale factor, lattice parameters, atomic positions, and profile parameters were refined in sequence until acceptable reliability factors (R_p = 10.06%, R_{wp} = 8.64%, R_{exp} = 3.44%) were achieved. The refinement result is demonstrated in Figure 3, and a clear match can be seen between the experimental and calculated profiles. The refined lattice parameters were calculated as $a = b$ = 10.4385 Å and c = 4.9674 Å and summarized in Supplementary Materials Table 1 along with the atomic coordinates. Along the crystallographic [1$\bar{1}$0] direction, an HRTEM image (**Figure 4a**) and the associated SAED pattern (**Figure 4b**) were obtained, revealing well-defined crystalline fringes with lattice spaces of 5.1 and 7.4 corresponding to lattice planes (001) and (110), respectively.

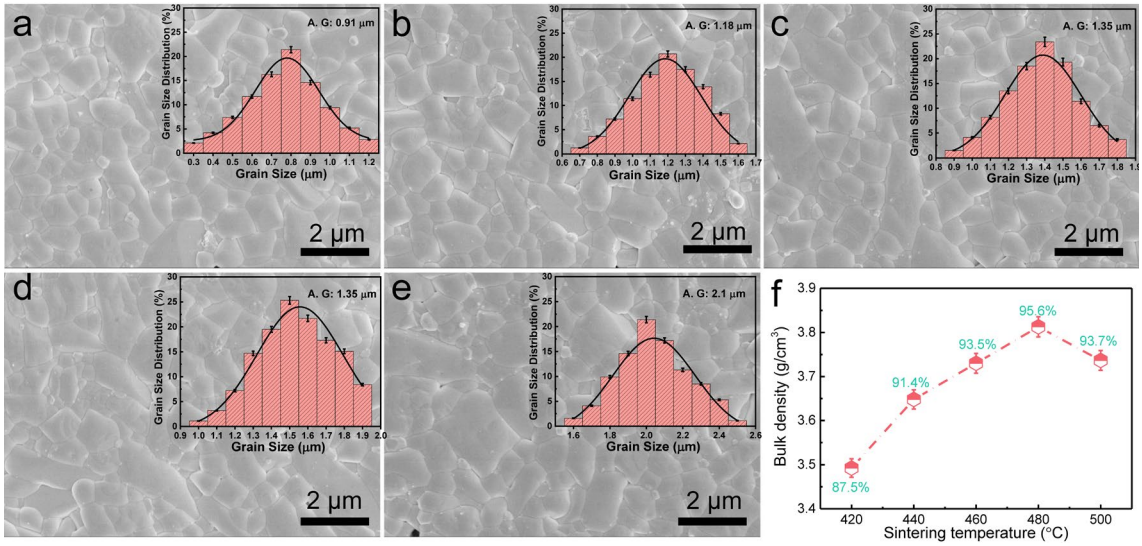

Figure 5

SEM images and grain size distribution of $Ag_2CaV_4O_{12}$ ceramics sintered at various temperatures are shown in **Figure 5**. Image analysis software revealed dense microstructures with tiny grain sizes ranging from 0.91 m to 2.1 m in all samples (Nano Measurer). No noticeable variations in particle size and morphology were found as the sintering temperature increased from 440 to 480 °C, indicating that the extrinsic effect of grain size on dielectric properties could be ruled out.

The bulk density and microwave dielectric characteristics of $Ag_2CaV_4O_{12}$ ceramics as a function of sintering temperature are shown in **Figure 6a-d**. The calculated theoretical density of $Ag_2CaV_4O_{12}$ was 3.99 g/cm^3. **Figure 6a** shows the bulk density which increased monotonously from ~ 87.5% of the theoretical density (3.49 g/cm^3) at 420 °C to ~ 95.6% of the theoretical density (3.81 g/cm^3) at 480 °C, depicting the highest relative density at this temperature. Upon further increasing the sintering temperature to 500 °C, the bulk density of the samples started to decrease, giving an optimum sintering temperature of $Ag_2CaV_4O_{12}$ to be 480 °C. The enhanced density is due to the grain growth, which agrees well with the microstructure evolution. Several other materials in literature, such as $Sr_3V_2O_8$, $Ba_2CuGe_2O_7$, Li_2ZnGeO_4, $AgPb_2Mg_2V_3O_{12}$ have also demonstrated similar phenomena.[15, 20-23].

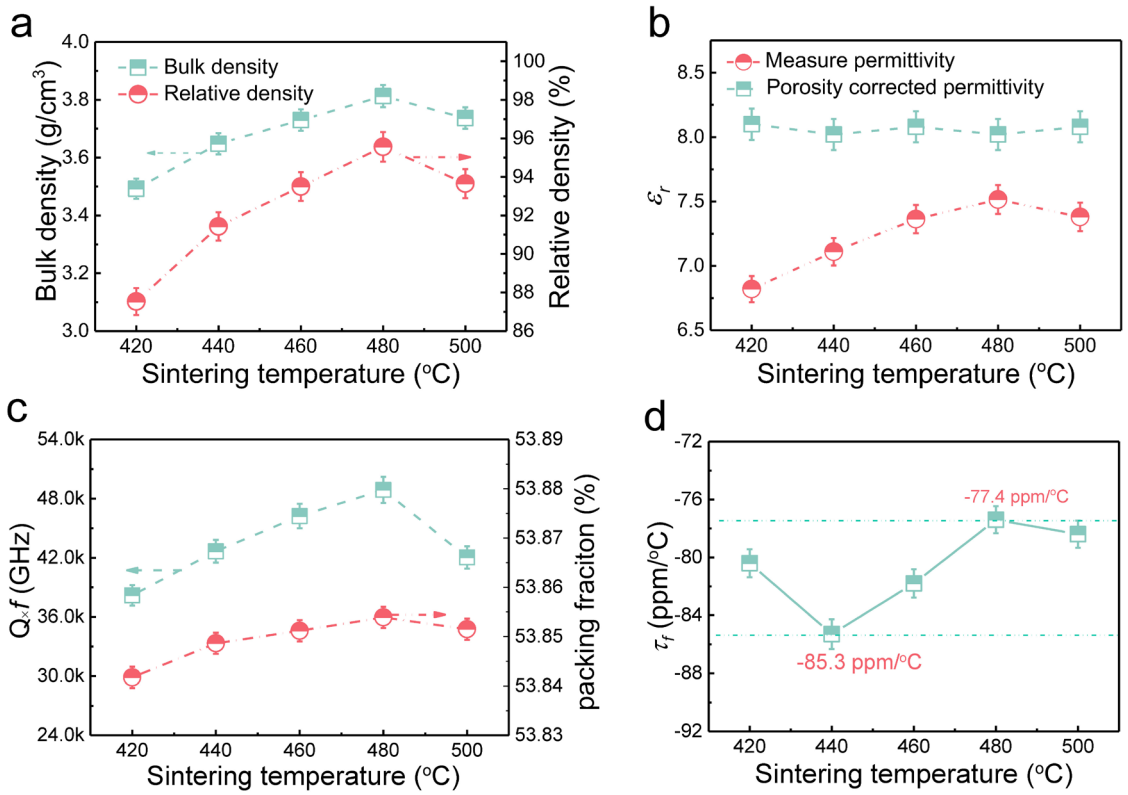

Figure 6

The variations in the relative permittivity (ε_r) follow the same trend as the density reaching a peak value at 480 °C before decreasing. It is generally accepted that that intrinsic and extrinsic factors such as the porosity, secondary phase, and grain boundaries control microwave dielectric properties [25-29]. The corrected permittivity (ε_{corr}) was calculated using the Bosman and Having's equation to exclude the influence of porosity on the permittivity, which is given in the equation below [30]:

$$\varepsilon_{corr} = \varepsilon_r(1+1.5p) \qquad (3)$$

where p represents the fractional porosity. The calculated ε_{corr} values, as shown in **Figure 6b**, are higher than the measured permittivity with a minimal deviation of 6.7% between them. It should be noticed that the corrected permittivity varies very little with sintering temperature, showing that density has a dominant effect on relative permittivity. Furthermore, we infer that the calculated ε_{corr} value should approach the intrinsic relative permittivity value, given the features of single-phase and similar grain

size. To confirm this hypothesis, the Clausius-Mossotti equation was used to calculate the theoretical permittivity [31-32]:

$$\varepsilon_{th} = \frac{3V_m + 8\pi\alpha_D^T}{3V_m - 4\pi\alpha_D^T} \quad (4)$$

$$\alpha_D^T = 2\alpha(Ag^+) + \alpha(Ca^{2+}) + 4\alpha(V^{4+}) + 12\alpha(O^{2-}) \quad (5)$$

where V_m represents the mole volume of the primitive unit cell; α_D^T is the total ionic polarizability of individual ions, can be obtained from the rule of mixture (eq. 4). For the sample sintered at 480 °C, α_D^T value was calculated to be 43.46 Å^3 using the above equation, through which the ε_{th} was calculated and gave a value of 7.16 [31]. The ε_{th} value is moderately lower than the measured value (ε_r ~7.52) which can be attributed to the "rattling" or "compressed" cations [31]. In this system, the movement of the ions leads to polyhedral distortions, causing increased ion polarizabilities and the permittivity of $Ag_2CaV_4O_{12}$ ceramics. By comparison with the estimated dielectric properties as given above, it is found that the calculated permittivity (7.05) value is slightly lower than that (7.52) measured at the microwave range, which could be attributed to the extrinsic contributions [33]. Additionally, the optical permittivity (1.83) only contributes to 25.9% of the total permittivity (7.05), which indicates that the ionic polarization was the primary contribution to the microwave dielectric properties rather than electronic [31].

The change in quality factors ($Q\times f$) as a function of sintering temperature is shown in **Figure 6c**. As the sintering temperature increased from 420 to 480 °C, the $Q\times f$ (at 13.6 GHz) values progressively increased from 38,100 to 48,800 GHz, then decreased with the increasing sintering temperature. Both intrinsic factors, such as lattice vibration mode, packing fraction, and also the extrinsic factors including the grain morphology, second phase, or porosity play a vital role in quality factor [26]. No secondary phase was discovered in sintered samples, as evidenced by XRD patterns, and all samples

have similar grain sizes. Since the quality factor follows the same trends of density, it is anticipated that the density has the primary effect on the quality factor compared to other external factors. However, the intrinsic contributions from structural features to the $Q\times f$ value can be described by the packing fraction, which is given as [34-36]:

$$\text{Packing fraction} = \frac{\text{the volume of packed ions}}{\text{the volume of a unit cell}} \times Z$$

$$= \frac{{}^{4\pi}/_{3}\times(2\times r_{Ag}^{3}+r_{Ca}^{3}+4\times r_{V}^{3}+12\times r_{O}^{3})}{V} \times Z \qquad (6)$$

where r represents the effective ion radii; V is the volume of a primitive unit cell and Z is the number of formula units per unit cell which has a value of 2 in the current system. Furthermore, when plotted against sintering temperature, the trend of packing fraction as a function of sintering temperature is comparable to that of the quality factor (**Figure 6c**). A higher packing fraction corresponds to a lower lattice vibration, leading to the lower dielectric loss and the higher quality factor. The theoretical quality factor was calculated to be 83,500 GHz, nearly double the measured $Q\times f$ value (48,800 GHz). Processing concerns, such as density, pore size, and grain size, can all contribute to such a huge variance.

As a function of sintering temperature, Figure 6d displays the temperature coefficient of resonance frequency (τ_f) values. The τ_f values float between -77.4 and -85.3 ppm/°C and are unaffected by the sintering temperature. To sum up, with ε_r 7.52, Qxf 48,800 GHz, and τ_f -77.4 ppm/°C, the $Ag_2CaV_4O_{12}$ ceramic sintered at 480 °C exhibits the best microwave dielectric characteristics.

The IR reflectivity spectrum can be used to estimate the inherent microwave dielectric characteristics of $Ag_2CaV_4O_{12}$ ceramic [37-40]. The contribution of lattice vibration to dielectric characteristics in the microwave band can be extrapolated by fitting the infrared reflection spectrum with the Kramers-Kronig (K-K) transform. Only the contribution of ionic and electronic displacement

polarisation is considered in the permittivity, which should be consistent with the measured value in the microwave frequency region. Extrapolated dielectric loss is commonly referred to as an inherent dielectric loss. As shown in **Figure 7**, the measured data were fitted using a classical harmonic oscillator that was modeled as follows:

$$R(\omega) = \left| \frac{\sqrt{\varepsilon^*(\omega)} - 1}{\sqrt{\varepsilon^*(\omega)} + 1} \right|^2 \tag{7}$$

$$\begin{aligned} \varepsilon^*(\omega) &= \varepsilon'(\omega) - i\varepsilon''(\omega) \\ &= \varepsilon_\infty + \sum_{j=1}^{n} \frac{S_j(\omega_j^2 - \omega^2)}{(\omega_j^2 - \omega^2)^2 + \omega^2\gamma^2} - i\sum_{j=1}^{n} \frac{S_j\omega\gamma_j}{(\omega_j^2 - \omega^2)^2 + \omega^2\gamma^2} \end{aligned} \tag{8}$$

where n denotes the order of transverse polar-phonon modes; ω_j, S_j, and j_γ is the frequency, strength, and damping constant of the j-th mode; and ε_∞ is the electronic polarization induced relative permittivity. When the ω meet the conditions of $\omega << \omega_j$, equations (6 and 7) are feasible:

$$\varepsilon'(\omega) = \varepsilon_\infty + \sum_{j=1}^{n} \Delta\varepsilon_j' = \varepsilon_\infty + \sum_{j=1}^{n} \frac{\omega_{pj}}{\omega_{oj}^2} \tag{9}$$

$$\varepsilon''(\omega) \approx \sum_{j=1}^{n} \frac{\omega_{pj}^2\gamma_j}{\omega_{oj}^2}\omega \tag{10}$$

$$\tan\delta = \frac{\varepsilon''}{\varepsilon'} = \sum_{j=1}^{n} \frac{S_j\omega\gamma_j}{\varepsilon'(\omega)\omega_j^4} \tag{11}$$

There are 15 modes employed in the $Ag_2CaV_4O_{12}$ ceramic, and comprehensive information on the fitted parameters is presented in Table 1. The dielectric characteristics are primarily influenced by these modes at 88.61 cm^{-1}, 183.97 cm^{-1}, and 200.4 cm^{-1}. Real and imaginary parts of the complex permittivity are shown in **Figure 7**. Based on the fitted parameters, the calculated permittivity at optical range (ε_∞) is 1.83 with a permittivity of 7.05 at microwave frequency. The theoretical quality factor was fitted to be 83,500 GHz.

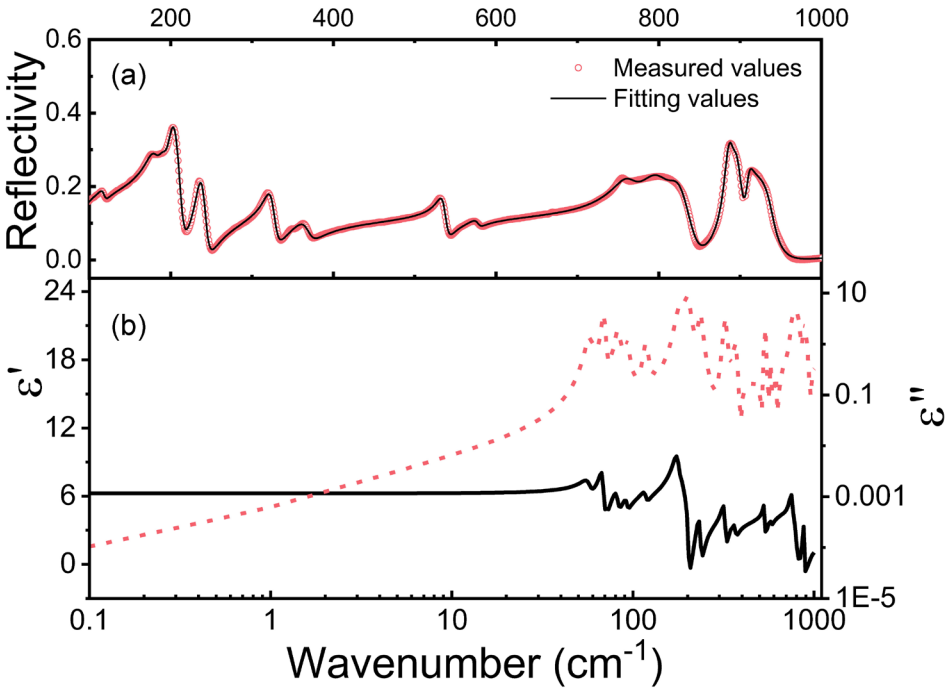

Figure 7

For practical application of microwave dielectric ceramics, the materials have to follow certain properties out of which one of the requirements is to have the $|\tau_f|$ values lower than 10 ppm/°C to guarantee the thermal stability of resonance frequency. To regulate/optimize the τ_f values to near zero, researchers have primarily used two strategies. The first way is to combine certain materials with positive τ_f values, such as TiO_2 (τ_f = +450 ppm/°C) and $CaTiO_3$ (τ_f = +800 ppm/°C) to make composite ceramics. The second strategy is to tune the τ_f values to near zero by forming a solid solution through doping or substitution. To modify the τ_f values, TiO_2 was used to create a composite with the composition $(1-x)Ag_2CaV_4O_{12-x}TiO_2$ (x = 0.1, 0.2, 0.3, 0.4, 0.5, 0.6).

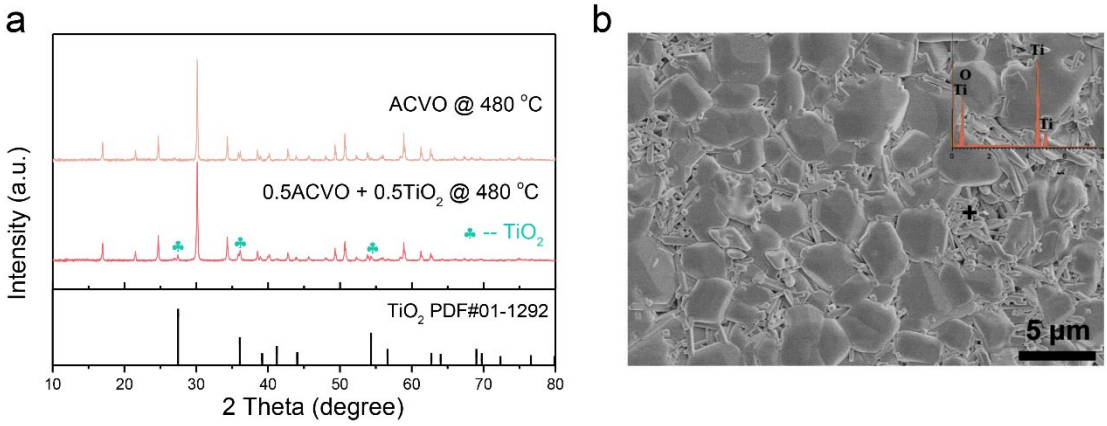

Figure 8

To assess the formation of composite, XRD was performed on the $0.5Ag_2CaV_4O_{12}$-$0.5TiO_2$ ceramic sintered at 480 °C for 6 hours. As demonstrated in **Figure 8a**, all of the peaks in the compound were matched to two phases: $Ag_2CaV_4O_{12}$ and TiO_2. There was no additional phase that could be seen, indicating that there was no chemical reaction between $Ag_2CaV_4O_{12}$ and TiO_2. EDS examination reveals that the small grains correspond to the TiO_2 phase, whereas the bigger grain is the matrix $Ag_2CaV_4O_{12}$, as shown in **Figure 8b**. Table 2 shows the microwave dielectric characteristics of $((1-x)Ag_2CaV_4O_{12-x}TiO_2)$ composite ceramics sintered at their optimal temperature (480 °C). Because of the higher permittivity of TiO_2 ($\varepsilon_r \sim 105$), the permittivity gradually increased with increasing x.[41]. The permittivity of the mixture phases was calculated using equation 6 and shown in **Table 2**, which were similar to measured values. Composites sintered at 500 °C with $x = 0.5$, optimum microwave dielectric properties were achieved which are given as $\varepsilon_r \sim 10.96$, $Q \times f \sim 49{,}081$ GHz, and a near-zero $\tau_f \sim 3.21$ ppm/°C.

$$\varepsilon_r = V_1 \lg \varepsilon_1 + V_2 \lg \varepsilon_2 \qquad (12)$$

Microwave dielectric properties of some low-firing ceramics are listed in **Table 3** [41-53]. The Majority of the compositions show good microwave dielectric properties together with low densification temperatures (< 960 °C). Generally, borates, silicates, and phosphates possess low

relative permittivity, e.g., $Li_3AlB_2O_6$ with the lowest $\varepsilon_r \sim 4.9$, whereas high relative permittivity is shown in those containing titanium and terbium. By comparison, the present $Ag_2CaV_4O_{12}$ has the lowest sintering temperature (480 °C) and competitive microwave dielectric properties, which renders an enormous potential in the ULTCC field.

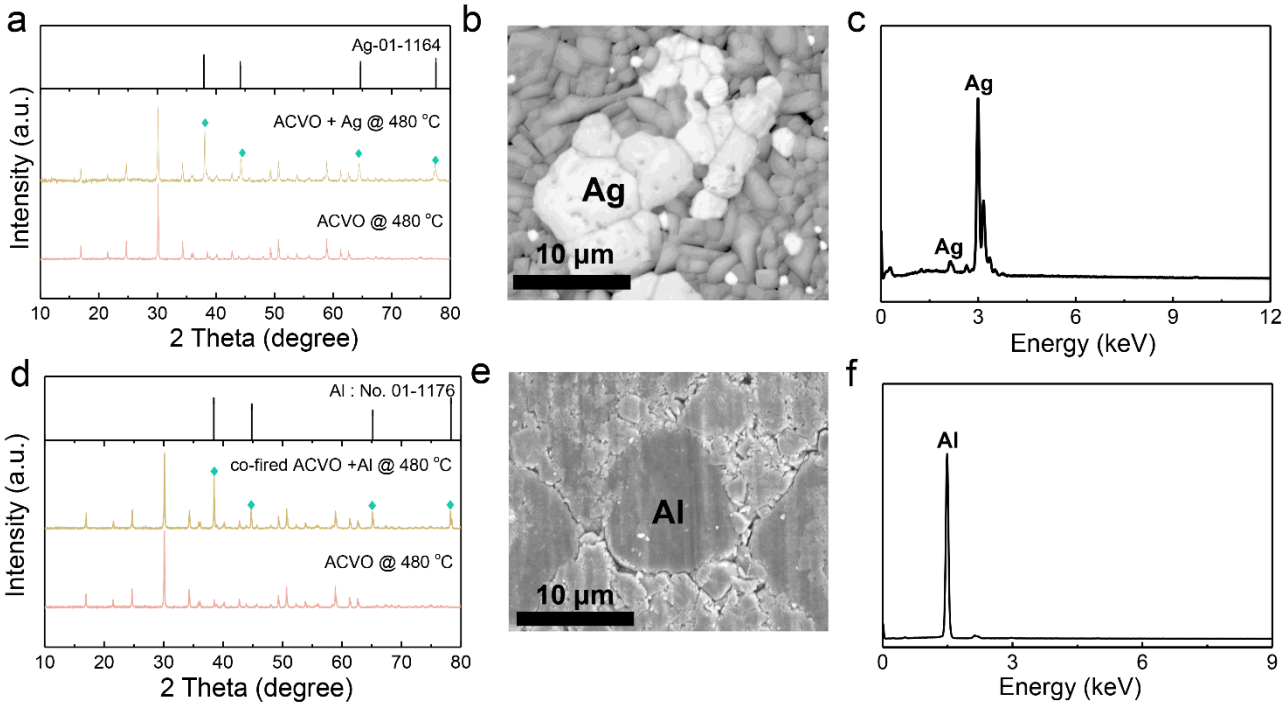

Figure 9

Because $Ag_2CaV_4O_{12}$ has a sintering temperature substantially lower than the melting points of Ag (961 °C) and Al (660 °C) electrodes, it has the potential to be used in LTCC and ULTCC technologies as it doesn't react with the electrode material. Co-firing with Ag and Al (in 20 wt. percent) was done by sintering at 480 °C to test the chemical compatibility of $Ag_2CaV_4O_{12}$ with Ag and Al electrodes. XRD patterns only indicated the diffraction peaks of $Ag_2CaV_4O_{12}$ and Ag/Al with no intermediate confirming the lack of reaction between the $Ag_2CaV_4O_{12}$ and Ag/Al as shown in **Figure 9 a&d**. During the microstructural examination using SEM, two types of grains with varied sizes and morphologies were observed as can be seen in **Figure 9 b&e**. The smaller grains were found to be $Ag_2CaV_4O_{12}$ phase by EDS analysis, while the larger bulk grains were Ag/Al as shown in **Figure 9 c&f**. The chemical

compatibility between $Ag_2CaV_4O_{12}$ and Ag/Al was proven by the above results, confirming the potential utilization of $Ag_2CaV_4O_{12}$ in LTCC and ULTCC applications.

Conclusions

In this paper, we presented a novel $Ag_2CaV_4O_{12}$ ceramic and its composite with TiO_2 with excellent microwave dielectric properties. These compositions could be easily synthesized via the conventional solid-state approach at extremely low temperatures (~ 50 °C) which is vital to demonstrate the chemical compatibility with common electrode materials such as Ag and Al where phase purity was examined through Rietveld refinement. Density variation and microstructure evaluation revealed a dense ceramic being sintered at 480 °C, exhibiting optimum microwave dielectric properties such as a low relative permittivity (ε_r) of 7.52 and a high quality factor ($Q\times f$) of 48,800 GHz. The large negative temperature coefficient of resonance frequency (τ_f) of -77.4 ppm/°C was reduced to a positive value of ~ 3.2 ppm/°C upon combining with rutile TiO_2 (60mol%), which inherently possesses a positive τ_f value, with almost no drift of resonance frequency was achieved. Hence, somewhat balanced microwave dielectric properties with an ε_r~ 10.96, a τ_f ~ 3.2 ppm/°C, and a $Q\times f$ ~ 49,081 GHz were achieved. No chemical reactions between $Ag_2CaV_4O_{12}$ and Ag/Al were confirmed through XRD and EDS analysis. All results demonstrate the potential applications of $Ag_2CaV_4O_{12}$ as dielectric resonances in wireless communications and substrates in low-temperature cofired ceramics. The ultralow temperature processing of $Ag_2CaV_4O_{12}$ shows that it is extraordinarily energy saving from the point of view of fabrication and might allow for room-temperature synthesis by combining with high-energy mechanical milling or sintering using high pressure such as hot isostatic pressing (HIP), spark plasma sintering (SPS), and cold sintering (CS).

Supporting Information

- **Table S1** Wyckoff position and refined atomic fractional coordinates from Rietveld refinement for $Ag_2CaV_4O_{12}$ with a space group *P4/nbm*
- **Figure S1** XRD patterns of $Ag_2CaV_4O_{12}$ sintered at 50 ºC, 100 ºC, and 150 ºC
- **Figure S2** Room temperature Raman spectra of $Ag_2CaV_4O_{12}$ ceramics sintered at different temperatures

Acknowledgments

The authors would like to thank the financial assistance from the Natural Science Foundation of China (No. 62061011), the National Key Research and Development Plan of China (No. 2017YFB0406300), the high-level innovation team, and the outstanding scholar program of Guangxi institutes. The authors would also like to express their gratitude to the officials in the IR beamline workstation of the National Synchrotron Radiation Laboratory (NSRL) for their assistance in the IR measurement.

Table 1 Phonon parameters obtained from the fitting of the infrared reflectivity spectra of the $Ag_2CaV_4O_{12}$ ceramic

Mode	ω_{oj} (cm^{-1})	ω_{pj} (cm^{-1})	γ_j (cm^{-1})	$\Delta\varepsilon_j$
1	69.41	31.77	0.409	0.0588
2	82.4	26.4	0.303	0.0826
3	88.61	79.95	0.814	0.107
4	183.97	152.45	0.687	0.128
5	200.4	136.81	0.566	0.0668
6	235.71	102.26	0.388	0.0507
7	322.46	127.57	0.156	0.0469
8	366.38	91.951	0.163	0.0538
9	484.11	235.55	0.337	0.845
10	534.33	129.93	0.0591	0.0225
11	597.86	184.58	0.0953	0.248
12	762.74	144.47	0.0359	0.0271
13	804.57	578.37	0.617	0.099
14	866.24	348.6	0.562	0.093
15	909.28	144.69	0.0253	0.0479
	$\varepsilon_\infty = 1.83$		$\varepsilon_r = 7.05$	

Table 2 Sintering temperature (S.T.) and microwave dielectric properties of (1-x)$Ag_2CaV_4O_{12}$-$x$$TiO_2$ composite ceramics

x	S.T. (°C)	ε_r	ε_{cal}	$Q\times f$ (GHz)	τ_f (ppm/°C)
0.1	480	7.76	7.81	48,915	-70.9
0.2	480	7.94	7.99	48,926	-62.8
0.3	490	8.32	8.24	48,954	-52.6
0.4	500	8.91	8.89	48,972	-40.3
0.5	500	9.55	9.68	49,021	-23.7
0.6	520	10.96	10.99	49,081	3.2

Table 3 Ceramics with low sintering temperature and competitive microwave dielectric properties

Ceramic	S. T. (°C)	Microwave dielectric properties			Reference
		ε_r	$Q\times f$ (GHz)	τ_f (ppm/°C)	
$Li_3AlB_2O_6$	700	4.9	12,609	-201	40
$NaAlSi_3O_8$	1025	5.5	11,200	-5	41
$K_{0.9}Ba_{0.1}Ga_{1.1}Ge_{2.9}O_8$	990	5.9	94,100	-25	42
50wt%Al_2O_3-50wt% SiO_2-B_2O_3-Al_2O_3	875	6.2	11,400	-35	43
$KGaGe_3O_8$	970	6.2	19,800	-21	44
$Mg_3(VO_4)_2$	950	6.4	48,800	-83	45
$Ba_2V_2O_7$	950	7.0	19,000	-74	46
$SrZnP_2O_7$	925	7.25	71,520	-64	47
$CaZnP_2O_7$	900	7.56	63,100	-82	47
Li_2O-B_2O_3-SiO_2-Al_2O_3-CaO	550	8	2,400	-48	48
$BaTi_4O_9$+B_2O_3-ZnO-La_2O_3 glass	900	27	20,000	6.5	49
$Ba_2Ti_9O_{20}$+3wt-%B_2O_3	940	28.3	10,800	-8.2	50
$Bi_2Te_2O_8$	650	39	23,000	-43	51
$TiTe_3O_8$	720	50	30600	133	52
$Ag_2CaV_4O_{12}$	480	7.52	48,800	-77.4	This work

Figure captions:

Figure 1 (a, c) structural diagrams projected along [100] and [001]; (b) coordination polyhedrons for cations.

Figure 2 XRD patterns of $Ag_2CaV_4O_{12}$ powders calcined at different temperatures.

Figure 3 Rietveld refinement on XRD data of the sample sintered at 480 °C.

Figure 4 (a) HRTEM image and (b) the corresponding SAED pattern of $Ag_2CaV_4O_{12}$ along the crystallographic [$1\bar{1}0$] direction.

Figure 5 SEM images and grain size distribution of $Ag_2CaV_4O_{12}$ ceramics sintered at different temperatures: (a) 420 ºC; (b) 440 ºC; (c) 460 ºC; (d) 480 ºC; (e) 500 ºC.

Figure 6 Variations in the (a) density, (b) relative permittivity, (c) quality factor, and (d) temperature coefficient of the resonance frequency of $Ag_2CaV_4O_{12}$ ceramics as a function of sintering temperature.

Figure 7 (a) IR reflectivity spectrum of $Ag_2CaV_4O_{12}$; (b) the fitted real and imaginary parts of the complex permittivity based on the Kramers-Kronig relationship.

Figure 8 (a) XRD patterns and (b) EDS analysis of $0.5Ag_2CaV_4O_{12}$ -$0.5TiO_2$ ceramic sintered at 480 °C for 6 h.

Figure 9 XRD patterns, SEM images, and EDS analysis of the co-fired $Ag_2CaV_4O_{12}$ with a silver (a, b, c) and with aluminum (d, e, f).

References

1 Sebastian, M. T. Dielectric materials for wireless communication. Elsevier Publishers: Oxford, U.K., 2008, 1-10.

2 Sebastian, M. T.; Jantunen, H. Low loss dielectric materials for LTCC applications: a review. *Int. Mater. Rev.* **2008,** *53* (2), 57-90.

3 Du, M. K.; Li, L. X.; Ni, L. Z.; Zhan, Y. Ultra-high Q $Ba(Mg_{1/3}Ta_{0.675})O_3$ microwave dielectric ceramics realized by slowly cooling step process and the simulation design for hairpin dielectric filters. *Ceram. Int.* **2021,** *47* (14), 19716-19726.

4 Ni, L. Z.; Li, L. X.; Du, M. K.; Zhan, Y. Wide temperature stable $Ba(Mg_xTa_{2/3})O_3$ microwave dielectric ceramics with ultra-high-Q applied for 5G dielectric filter. *Ceram. Int.* **2021,** *47* (1), 1034-1039.

5 Lin, Q. B.; Song, K. X.; Liu, B.; Bafrooei, H. B.; Zhou, D.; Su, W. T.; Shi, F.; Wang, D. W.; Lin, H. X.; M.Reaney, I. Vibrational spectroscopy and microwave dielectric properties of $AY_2Si_3O_{10}$ (A = Sr, Ba) ceramics for 5G applications. *Ceram. Int.* **2020,** *46* (1), 1171-1177.

6 Zhou, D.; Pang, L. X.; Wang, D. W.; Li, C.; Jin, B. B.; Reaney, I. M. High permittivity and low loss microwave dielectrics suitable for 5G resonators and low temperature co-fired ceramic architecture. *J. Mater. Chem. C* **2017,** *5* (38), 10094-10098.

7 Zhang, J.; Zuo, R. Z.; Wang, Y.; Qi, S. S. Phase evolution and microwave dielectric properties of $Li_4Ti_{5(1+x)}O_{12}$ ceramics. *Mater. Lett.* **2016,** *164*, 353-355.

8 Zhang, J.; Zuo, R. Z. Effect of Ordering on the Microwave Dielectric Properties of Spinel-Structured $(Zn_{1-x}(Li_{2/3}Ti_{1/3})_x)_2TiO_4$ Ceramics. *J. Am. Ceram. Soc.* **2016,** *99* (10), 3343-3349.

9 Zhou, H. F.; Liu, X. B.; Chen, X. L.; Fang, L. Preparation, phase structure and microwave dielectric properties of a new low cost $MgLi_{2/3}Ti_{4/3}O_4$ compound. *Mater. Chem. Phys.* **2012,** *137* (1), 22-25.

10 Ma, J. L.; Fu, Z. F.; Liu, P.; Wang, B.; Li, Y. Microwave dielectric properties of low-fired Li_2TiO_3-MgO ceramics for LTCC applications. *Mater. Sci. Eng. B* **2016,** *204*, 15-19.

11 Subodh, G.; Sebastian, M. T. Glass-free $Zn_2Te_3O_8$ microwave ceramic for LTCC applications. *J. Am. Ceram. Soc.* **2010,** *90* (7), 2266-2268.

12 Xing, C. F.; Bao, J.; Sun, Y. F.; Sun, J. J.; Wu, H. T. Ba_2BiSbO_6: A novel microwave dielectric ceramic with monoclinic structure. *J. Alloys Compd.* **2019,** *782*, 754-760.

13 Pang, L. X.; Zhou, D.; Wang, D. W.; Zhao, J. X.; Liu, W. G.; Yue, Z. X.; Reaney, I. M. Temperature stable $K_{0.5}(Nd_{1-x}Bi_x)_{0.5}MoO_4$ microwave dielectrics ceramics with ultra-low sintering temperature. *J. Am. Ceram. Soc.* **2018,** *101* (5), 1806-1810.

14 Yin, C. Z.; Li, C. C.; Yang, G. J.; Fang, L.; Yuan, Y. H.; Shu, L. L.; Khaliq, J. $NaCa_4V_5O_{17}$: A low-firing microwave dielectric ceramic with low permittivity and chemical compatibility with silver for LTCC applications. *J. Eur. Ceram. Soc.* **2020,** *40* (2), 386-390.

15 Madhuri, R.; Ganesanpotti, S. Crystal structure, phonon modes, and bond characteristics of $AgPb_2B_2V_3O_{12}$ (B = Mg, Zn) microwave ceramics. *J. Am. Ceram. Soc.* **2020,** *103* (5), 3157-3167.

16 Zhou, D.; Pang, L. X.; Wang, D. W.; Qi, Z. M.; Reaney, I. M. High Quality Factor, Ultralow Sintering Temperature $Li_6B_4O_9$ Microwave Dielectric Ceramics with Ultralow Density for Antenna Substrates. *ACS Sustainable Chem. Eng.* **2018,** *6* (8), 11138-11143.

17 Yin, C. Z.; Xiang, H. C.; Li, C. C.; Porwal, H.; Fang, L. Low-temperature sintering and thermal stability of Li_2GeO_3-based microwave dielectric ceramics with low permittivity. *J. Am. Ceram. Soc.* **2018,** *101* (10), 4608-4614.

18 Lu, Y. J.; Wan, Y. P.; Bi, S. L.; Weng, H. G.; Huang, Y. L.; Qin, L.; Seo, H. J. Synthesis, surface and optical properties of $Ag_2CaV_4O_{12}$ nanoparticles for dye removal under visible irradiation. *Mater. Chem. Phys.* **2016,** *180*, 263-271.

19 Hakki, B.W.; Coleman, P. D. A dielectric resonant method of measuring inductive capacitance in the millimeter range.

IEEE Trans. Microw. Theory Tech. **1960,** *8,* 401-410.

20 Yin, C. Z.; Yu, Z. Z.; Shu, L. L.; Liu, L. J.; Chen, Y.; Li, C.C. A low-firing melilite ceramic $Ba_2CuGe_2O_7$ and compositional modulation on microwave dielectric properties through Mg substitution. *J. Adv. Ceram.* **2021,** *10* (1), 108-119.

21 Cheng, K.; Li, C. C.; Yin, C.C.; Tang, Y.; Sun, Y. H.; Fang, L. Effects of Sr^{2+} substitution on the crystal structure, Raman spectra, bond valence and microwave dielectric properties of $Ba_{3-x}Sr_x(VO_4)_2$ solid solutions. *J. Eur. Ceram. Soc.* **2019,** *39* (13), 3738-3743.

22 Li, C. C.; Yin, C. Z.; Deng, M.; Shu, L. L.; Khaliq, J. Tunable microwave dielectric properties in $SrO\text{-}V_2O_5$ system through compositional modulation. *J. Am. Ceram. Soc.* **2019,** *103* (4), 2315-2321.

23 Li, C. C.; Xiang, H. C.; Xu, M. Y.; Tang, Y.; Fang, L. Li_2AGeO_4 (A = Zn, Mg): Two novel low-permittivity microwave dielectric ceramics with olivine structure. *J. Eur. Ceram. Soc.* **2018,** *38* (4), 1524-1528.

24 Kim, W. S.; Kim, E. S.; Yoon, K. H. Effects of Sm^{3+} Substitution on Dielectric Properties of $Ca_{1-x}Sm_{2x/3}TiO_3$ Ceramics at Microwave Frequencies. *J. Am. Ceram. Soc.* **2004,** *82* (8), 2111-2115.

25 Kim, E. S.; Chun, B. S.; Yoon, K. H. Dielectric properties of $[Ca_{1-x}(Li_{1/2}Nd_{1/2})_x]_{1-y}Zn_yTiO_3$ ceramics at microwave frequencies. *Mater. Sci. Eng. B* **2003,** *99* (1-3), 93-97.

26 Du, K.; Song, X. Q.; Li, J.; Wu, J. M.; Lu, W. Z.; Wang, X. C.; Lei, W. Optimised phase compositions and improved microwave dielectric properties based on calcium tin silicates. *J. Eur. Ceram. Soc.* **2019,** *39* (2), 340-345.

27 Zhou, D.; Pang, L. X.; Wang, D. W.; Guo, H. H.; Yang, F.; Qi, Z. M.; Li, C.; Jin, B. B.; Reaney, I. M. Crystal structure, impedance and broadband dielectric spectra of ordered scheelite-structured $Bi(Sc_{1/3}Mo_{2/3})O_4$ ceramic. *J. Eur. Ceram. Soc.* **2018,** *38* (4), 1556-1561.

28 Guo, H. H.; Zhou, D.; Pang, L. X.; Qi, Z. M. Microwave dielectric properties of low firing temperature stable scheelite structured (Ca, Bi)(Mo, V)O_4 solid solution ceramics for LTCC applications. *J. Eur. Ceram. Soc.* **2019,** *39*, 2365-2373.

29 Yoon, S. H.; Kim, D.; Cho, S.; Hong, K. S. Investigation of the relations between structure and microwave dielectric properties of divalent metal tungstate compounds. *J. Eur. Ceram. Soc.* **2006,** *26* (10), 2051-2054.

30 Shannon, R. D. Dielectric polarizabilities of ions in oxides and fluorides. *J. Appl. Phys.* **1993,** *73*, 348-366.

31 Shannon, R. D.; Rossman, G. R. Dielectric constants of silicate garnets and the oxide additivity rule. *Am. Mineral.* **1992,** *77* (1-2), 94-100.

32 Xiong, Y.; Xing, Z.; Weng, J. H.; Ma, C.; Khaliq, J.; Li, C. C. Low-temperature sintering, dielectric performance, and far-IR reflectivity spectrum of a lightweight $NaCaVO_4$ with good chemical compatibility with silver. *Ceram. Int.* **2021,** *47* (15), 22219-22224.

33 Kim, E. S.; Chun, B. S.; Freer, R.; Cernik, R. J. Effects of packing fraction and bond valence on microwave dielectric properties of $A^{2+}B^{6+}O_4$ (A^{2+}: Ca, Pb, Ba; B^{6+}: Mo, W) ceramics. *J. Eur. Ceram. Soc.* **2010,** *30* (7), 1731-1736.

34 Xiao, M.; Gu, Q. Q.; Zhou, Z. Q.; Zhang, P. Study of the microwave dielectric properties of $(La_{1-x}Sm_x)NbO_4$ (x = 0-0.10) ceramics via bond valence and packing fraction. *J. Am. Ceram. Soc.* **2017,** *100* (9), 3952-3960.

35 Liao, Q. W.; Li, L. X.; Xiang, R.; Xiang, D. New Low-loss Microwave Dielectric Material $ZnTiNb_2O_8$. *J. Am. Ceram. Soc.* **2011,** *94* (10), 3237-3240.

36 Zheng, C. W.; Fan, X. C.; Chen, X. M. Analysis of infrared reflection spectra of $(Mg_{1-x}Zn_x)$ Al_2O_4 microwave dielectric ceramics. *J. Am. Ceram. Soc.* **2008,** *91* (2), 490-493.

37 Spitzer, W. G.; Miller, R. C.; Kleinman, D. A.; Howarth, L. E. Far Infrared Dielectric Dispersion in $BaTiO_3$, $SrTiO_3$, and TiO_2. *Physical Review* **1962,** *126* (5), 1710-1721.

38 Guo, J.; Zhou, D.; Wang, L.; Wang, H.; Shao, T.; Qi, Z. M.; Yao, X. Infrared spectra, Raman spectra, microwave dielectric properties and simulation for effective permittivity of temperature stable ceramics $AMoO_4\text{-}TiO_2$ (A = Ca, Sr). *Dalton Trans.* **2013,** *42* (5), 1483-91.

39 Wakino, K.; Murata, M.; Tamura, H. Far Infrared Reflection Spectra of Ba(Zn, Ta)O_3-$BaZrO_3$ Dielectric Resonator Material. *J. Am. Ceram. Soc.* **1986,** *69* (1), 34-37.

40 Guo, J.; Zhou, D.; Wang, H.; Yao, X. Microwave dielectric properties of (1-*x*)$ZnMoO_4$-*x*TiO_2 composite ceramics. *J. Alloys Compd.* **2011,** *509* (19), 5863-5865.

41 Ohashi, M.; Ogawa, H.; Kan, A.; Tanaka, E. Microwave dielectric properties of low-temperature sintered $Li_3AlB_2O_6$ ceramic. *J. Eur. Ceram. Soc.* **2005,** *25* (12), 2877-2881.

42 Krzmanc, M. M.; Valant, M.; Suvorov, D.; A structural and dielectric characterization of $Na_xCa_{1-x}Al_{2-x}Si_{2+x}O_8$ (x = 0 and 1) ceramics. *J. Eur. Ceram. Soc.* **2005,** *25* (12), 2835-2838.

43 Krzmanc, M. M.; Meden; A.; Suvorov; D. The correlation between the structure and the dielectric properties of $K_xBa_{1-x}Ga_{2-x}Ge_{2+x}O_8$ ceramics. *J. Eur. Ceram. Soc.* **2007,** *27* (8-9), 2957-2961.

44 Choi, Y. J.; Park, J. H,; Ko, W. J.; Hwang, I. S.; Park, J. H.; Park, J. G.; Nahm, S.; Co-Firing and Shrinkage Matching in Low- and Middle- Permittivity Dielectric Compositions for a Low-Temperature Co-Fired Ceramics System. *J. Am. Ceram. Soc.* **2005,** *89* (2), 562-567.

45 Krzmanc, M. M.; Meden, A.; Suvorov, D. The correlation between the structure and the dielectric properties of $K_xBa_{1-x}Ga_{2-x}Ge_{2+x}O_8$ ceramics. *J. Eur. Ceram. Soc.* **2007,** *27* (8-9), 2957-2961.

46 Umemura, R.; Ogawa, H.; Ohsato, H.; Kan, A.; Yokoi, A. Microwave dielectric properties of low-temperature sintered $Mg_3(VO_4)_2$ ceramic. *J. Eur. Ceram. Soc.* **2005,** *25* (12), 2865-2870.

47 Umemura, R.; Ogawa, H.; Yokoi, A.; Ohsato, Hi.; Kan, A. Low-temperature sintering-microwave dielectric property relations in $Ba_3(VO_4)_2$ ceramic. *J. Alloys Compd.* **2006,** *424* (1-2), 388-393.

48 Bian, J. J.; Kim, D. W.; Hong, K. S. Glass-free LTCC microwave dielectric ceramics. *Mater. Res. Bull.* **2005,** *40* (12), 2120-2129.

49 Cho, I. S.; Kim, D. W.; Kim, J. R.; Hong, K. S. Low-temperature sintering and microwave dielectric properties of $BaO(Nd_{1-x}Bi_x)_2O_3 \cdot 4TiO_2$ by the glass additions. *Ceram. Int.* **2004,** *30* (7), 1181-1185.

50 Guan, E.; Chen, W.; Luo, L. Low firing and microwave dielectric properties of $BaTi_4O_9$ with B_2O_3–ZnO-La_2O_3 glass addition. *Ceram. Int.* **2007,** *33* (6), 1145-1148.

51 Lee, Y. C.; Lee, W. H.; Shieu, F. S.; Effects of B_2O_3 addition on the microwave dielectric properties of $Ba_2Ti_9O_{20}$ ceramics. *Jpn. J. Appl. Phys.* **2003,** *42* (3R), 1311.

52 Udovic, M.; Valant, M.; Suvorov, D. Phase formation and dielectric characterization of the Bi_2O_3-TeO_2 system prepared in an oxygen atmosphere. *J. Am. Ceram. Soc.* **2004,** *87* (4), 591-597.

53 Udovic, M.; Valant, M.; Suvorov, D. Dielectric characterisation of ceramics from the TiO_2-TeO_2 system. *J. Eur. Ceram. Soc.* **2001,** *21* (10-11), 1735-1738.

For Table of Contents Use Only

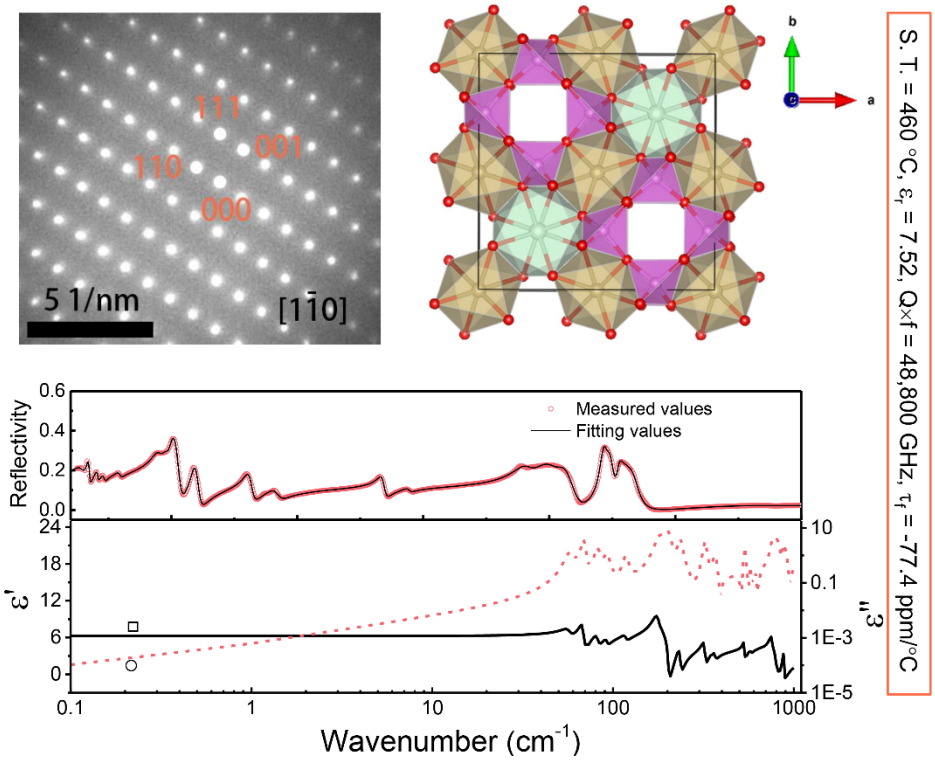

TEM, crystal structure, and far IR spectrum of Ag2CaV4O12 along with the microwave dielectric properties